SCIENCE CHINA Materials

ARTICLES

mater.scichina.com link.springer.com

Published online 30 August 2017 | doi: 10.1007/s40843-017-9083-9
Sci China Mater 2017, 60(9): 839–848

A novel lithium-ion battery comprising Li-rich@Cr_2O_5 composite cathode and $Li_4Ti_5O_{12}$ anode with controllable coulombic efficiency

Xiang Ding, Bangkun Zou, Yuxuan Li, Xiaodong He, Jiaying Liao, Zhongfeng Tang, Yu Shao and Chunhua Chen*

ABSTRACT **Through meticulous design, a Li-lacking Cr_2O_5 cathode is physically mixed with Li-rich $Li_{1.2}Ni_{0.13}Co_{0.13}Mn_{0.54}O_2$ (LNCM) cathode to form composite cathodes LNCM@xCr_2O_5 (x = 0, 0.1, 0.2, 0.3, 0.35, 0.4, mass ratio) in order to make use of the excess lithium produced by the Li-rich component in the first charge-discharge process. The initial coulombic efficiency (ICE) of LNCM half-cell has been significantly increased from 75.5% (x = 0) to 108.9% (x = 0.35). A novel full-cell comprising LNCM@Cr_2O_5 composite cathode and $Li_4Ti_5O_{12}$ anode has been developed. Such electrode accordance, i.e., LNCM@Cr_2O_5//$Li_4Ti_5O_{12}$ ("L-cell"), shows a particularly high ICE of 97.7%. The "L-cell" can transmit an outstanding reversible capacity up to 250 mA h g^{-1} and has 94% capacity retention during 50 cycles. It also has superior rate capacities as high as 122 and 94 mA h g^{-1} at 1.25 and 2.5 A g^{-1} current densities, which are even better in comparison of Li-rich//graphite full-cell ("G-cell"). The high performance of "L-cell" benefiting from the well-designed coulombic efficiency accordance mechanism displays a great potential for fast charge-discharge applications in future high-energy lithium ion batteries.**

Keywords: Li-rich cathode, chromium oxide, lithium titanium oxide, electrode accordance, rate capability

INTRODUCTION

Electric/hybrid and electric vehicles (EVs/HEVs) powered by lithium ion batteries (LIBs) have undergone tremendous development during these years, which also contribute to the rapidly increased demands on LIBs for their long cycle life, high energy density and guaranteed safety property [1–5]. However, the current commercial LIB cathode materials, such as $LiFePO_4$, $LiMn_2O_4$ and $LiCoO_2$ [6–8], are mainly restricted by their inferior specific capacity and resulting low energy density for the further applications in HEVs and EVs.

Li-rich layered oxides $\alpha Li_2MnO_3{\cdot}(1-\alpha)LiMO_2$ (M = Mn, Co, Ni, etc.) have drawn considerable heed as prospective cathode materials for their higher reversible specific capacity and energy density (more than 251 mA h g^{-1} and about 950 W h kg^{-1}) than the commercial cathode materials referred above [9,10]. However, these Li-rich electrodes have natural defects such as poor rate performance, gradual voltage decay and low initial coulombic efficiency (ICE, about 75%) [11,12]. Though the voltage decay and poor rate performance can be alleviated by taking some measures like lattice doping, surface coating and morphology design [13–21], the capacity fading (about 25%) caused by the irreversible transformation of Li_2MnO_3 phase in Li-rich from layered-structure to spinel-structure $LiMn_2O_4$ with the release of Li^+ and oxygen in the first cycle is practically unavoidable, which is a challenge for their applications in LIBs as before [22–24]. At present, ongoing research efforts mainly concentrate on conquering the large irreversible capacity loss counterbalanced by anode materials with similar percentage of initial irreversible capacity loss, such as carbon [25–27], transition metal oxides [28] and composite Si/C or Sn/C [29–31]. The continuous formation of solid electrolyte interphase (SEI) film on the anode electrode's surface and the trapping of some lithium in anode electrode crystal structure can lead to the irreversibility of Li^+ in LIBs. Nevertheless, they do not really succeed in transforming the originally irreversible lithium into usable reversible capacity in Li-rich half-cells and full-cells.

Herein, an innovative strategy is employed to solve the problem of the first charge-discharge capacity loss for Li-

CAS Key Laboratory of Materials for Energy Conversions, Department of Materials Science and Engineering & Collaborative Innovation Center of Suzhou Nano Science and Technology, University of Science and Technology of China, Hefei 230026, China
* Corresponding author (email: cchchen@ustc.edu.cn)

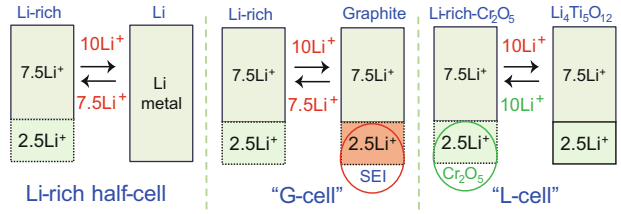

Figure 1 Schematic diagram of the "L-cell" coulombic efficiency accordance mechanism.

rich cathodes so as to get higher energy density in both half-cells and full-cells. We first synthesized Li-lacking Cr_2O_5 powders and Li-rich $Li_{1.2}Ni_{0.13}Co_{0.13}Mn_{0.54}O_2$ (LNCM) powders. Then the half-cell and full-cell tests were conducted. As shown in Fig. 1, the ICE is only about 75% in Li-rich half-cell. If we match Li-rich cathode with graphite anode to construct a full cell, the ICE of the "G-cell" is also about 75%, in which the irreversible lithium (about 25%) in the first cycle is caused by the activation of the Li-rich cathode and the simultaneous formation of SEI film on the graphite anode electrode [32]. It results in an insufficient use of lithium of Li-rich cathode. However, through simply physically mixing them with different mass ratios, the ICE was improved from 75.5% up to 112% in half-cell (*vs.* Li). Moreover, through matching with $Li_4Ti_5O_{12}$ anode (ICE = 94.9%), an ICE up to 97.7% has been achieved in the full-cell, which proves that Cr_2O_5 really effectively stores the extra irreversible Li^+ in Li-rich cathode. This "L-cell" can transmit a reversible capacity up to 251 mA h g^{-1} with 94% capacity retention during 50 cycles. Besides, its good rate capacity as high as 122 and 94 mA h g^{-1} at 1.25 and 2.5 A g^{-1} current densities, respectively, is much superior compared to a Li-rich//graphite full-cell matched up in this paper, which can be used in potential fast charge-discharge applications in EVs/HEVs.

EXPERIMENTAL SECTION

Electrode preparations

The Li-rich transition metal oxides LNCM cathode material was chemically synthesized by a citric acid auto-combustion method. Citric acid, $LiNO_3$ (5% excess), $Co(NO_3)_2{\cdot}6H_2O$, $Ni(NO_3)_2{\cdot}6H_2O$ and $Mn(CH_3COO)_2{\cdot}4H_2O$ with a calculated stoichiometric ratio (1.7:1.26:0.13:0.13:0.54) were dissolved in deionized water to form an aqueous solution of 0.4 mol L^{-1}. Aqueous ammonia was put into the solution to control the pH up to 7. Then, the aqueous solution was magnetically stirred for 4 h at room temperature. Next, the solution was heated at 250°C for 6 h in an electric oven to evaporate the solvent and followed by an auto-combustion. Afterwards, the mid-product material was transferred to a muffle stove and sintered at 500°C for 6 h to obtain a precursor. Finally, the precursor was sintered at 950°C for 10 h to obtain the Li-rich LNCM cathode material. These powders were ground in a crucible after each step. Separately, the Cr_2O_5 cathode material was prepared by a simple one-step solid phase decomposition method. CrO_3 was heated at 350°C for 2 h in air to obtain Cr_2O_5 powders. For the purpose of improving the ICE up to 100% in half-cell, different mass ratios of LNCM@Cr_2O_5 composites were designed according to this formula: $340m = 251m + 255xm$ (m and xm are the masses of the LNCM and Cr_2O_5, respectively), whose answer is $x = 0.35$. Thence, we performed $x = 0.1$, 0.2, 0.3, 0.35 and 0.4 as the basis for composing the LNCM@Cr_2O_5 composites. The LNCM@Cr_2O_5 composites were obtained by mechanically mixing the LNCM and Cr_2O_5 powders in the crucible. All the raw materials mentioned above were produced by Sinopharm Chemical Reagent Co., Ltd (ShangHai, China). Besides, a $Li_4Ti_5O_{12}$ powder (named LTO) and a graphite powder were purchased from ATL Amperex Technology Limited (NingDe, China).

Electrochemical examinations

Coin-cells (CR2032-type) were selected to test the electrochemical performances of all cells, which were assembled in an argon atmosphere glovebox (MBraun Labmaster 130). In half-cells, the cathode electrodes consisted of Li-rich (or Cr_2O_5 or LNCM@Cr_2O_5) powders, carbon black and polyvinylidene fluoride (PVDF) binder with a 7:2:1 mass ratio onto a current collector aluminium foil. Besides, the anode electrodes consisted of $Li_4Ti_5O_{12}$ (or graphite) powders, carbon black and PVDF binder with a 7:2:1 (or 90:3:7) mass ratio onto a current collector copper foil. A thin Celgard 2400 polypropylene film was selected to be the separator. A round lithium foil was chosen as the counter electrode. The electrolyte was 1 mol L^{-1} $LiPF_6$ solution in dimethyl carbonate (DMC) and ethylene carbonate (EC) as the solvent (1:1, *v*/*v*, Suzhou Electronics Materials Co. Ltd) in both half-cells and full-cells. The full cell consisted of an LNCM@Cr_2O_5 composite cathode electrode and a $Li_4Ti_5O_{12}$ anode electrode (or LNCM and graphite). The cathodes' mass rolling density in aluminium foil was 2.25 mg cm^{-2} in half-cell and full-cell. The mass rolling density of the anodes in copper foil was 1.15 g cm^{-2} in half-cell. Moreover, to make full use of the capacity of the cathode in full-cell, the anode electrodes ($Li_4Ti_5O_{12}$ and graphite) were prepared

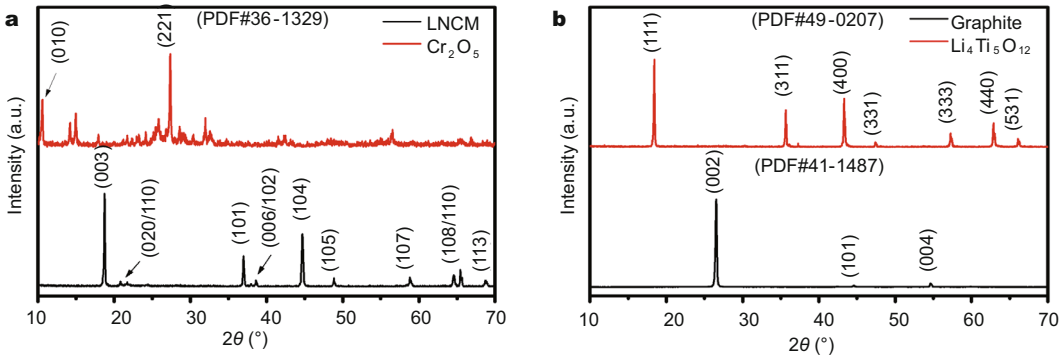

Figure 2 XRD patterns of (a) the synthesized powders Li-rich layer-structured LNCM and Cr_2O_5 cathodes and (b) $Li_4Ti_5O_{12}$ and graphite anodes, respectively.

with 10% excess capacity in order to make the cathode capacity control the full-cell capacity. Hence, the mass rolling density of the anodes in aluminium foil is 3.77 mg cm^{-2} for the $Li_4Ti_5O_{12}$ and 1.7 mg cm^{-2} for the graphite in full cells. The charge-discharge voltages are 0.5–2.96 V for LNCM@Cr_2O_5//$Li_4Ti_5O_{12}$ and 1.8–4.6 V for LNCM//graphite in full cells, which are 2.0–4.8 V for LNCM//lithium and Cr_2O_5//lithium in half cells. All the performances of half-cells and full-cells were gradually tested on a galvanostatical battery test system (Neware BTS-2300).

Characterization of electrode materials

The morphologies of cathode and anode materials were analyzed by using scanning electron microscopy (SEM, JSM-6390 LA, JEOL). X-ray diffraction (XRD, Rigaku TTR-III, Cu Kα radiation) was used to characterize the micro structure of cathode and anode materials.

RESULTS AND DISCUSSION

The synthesized Li-rich LNCM powder is identified as the α-$NaFeO_2$ structure (space group: *R*3*m*) without any impurities (Fig. 2a). The peaks located at 20° to 25° are considered to be the Li_2MnO_3 phase with a *C*2/*m* space group symmetry in a Li-rich structure. Meantime, the obvious splits located in (006)/(102) and (108)/(110) diffraction peaks indicate that the material is of good layered structure in lattice. The XRD patterns of Cr_2O_5 cathode material is also exhibited in Fig. 2a (PDF#36-1329). The sharp and clear diffraction peaks in Fig. 2b also clearly indicate a well crystalline $Li_4Ti_5O_{12}$ (space group: *Fd*-3*m*, PDF#49-0207) with a face-centered cubic spinel structure. The LNCM@Cr_2O_5 composite cathode materials with different *x* values are exhibited in Fig. S1. The diffraction peaks of Cr_2O_5 in LNCM@Cr_2O_5 composite materials become stronger with increased *x* value. It suggests that the physical mixing process does not change the structure of LNCM and Cr_2O_5 pristine materials.

The SEM images of these cathode and anode samples are illustrated in Fig. 3. The typical morphology of the LNCM (Fig. 3a) powders is uniformly distributed irregular spheres with a particle size of about 400 nm. In contrast, the morphology of the Cr_2O_5 powders (Fig. 3b) shows a range from 0.3 to 2 μm in particle size. The SEM images of the composite samples are demonstrated in Fig. S2a–d. After physical mixing with a given mass of Cr_2O_5, the morphologies of the powders become non-uniform with some large size particles distributed in LNCM powders, which corresponds to *x* values of 0.1, 0.2, 0.3 and 0.35 for the composites. For anode materials, the LTO sample has a particle size of about 400 nm from the SEM image (Fig. 3c). The graphite sample has a particle size of about 2.7 μm (Fig. 3d).

In order to reasonably fabricate the full cells, the electrochemical performances of the cathodes and anodes were investigated by half-cells (2.0–4.8 V *vs.* Li) firstly. The discharge capacity of LNCM is 251 mA h g^{-1} at 0.1 C with a 75.5% ICE (Fig. 4a), but the specific capacity is 210 mA h g^{-1} at 0.5 C initially and 183 mA h g^{-1} remained during 100 cycles with an 87% capacity retention percentage (Fig. 4b). It is worth mentioning that, the coulombic efficiency of LNCM is all nearly 100% except for the first cycle. The LNCM sample exhibits typical electrochemical charge-discharge behavior of a Li-rich cathode, while the charge slope below 4.4 V is accompanied with $Co^{3+/4+}$ and $Ni^{2+/4+}$ redox reactions and the charging plateau above 4.5 V is related to the activation of Li_2MnO_3 phase [33,34]. Besides, the LNCM cathode can provide an outstanding rate capability, whose reversible

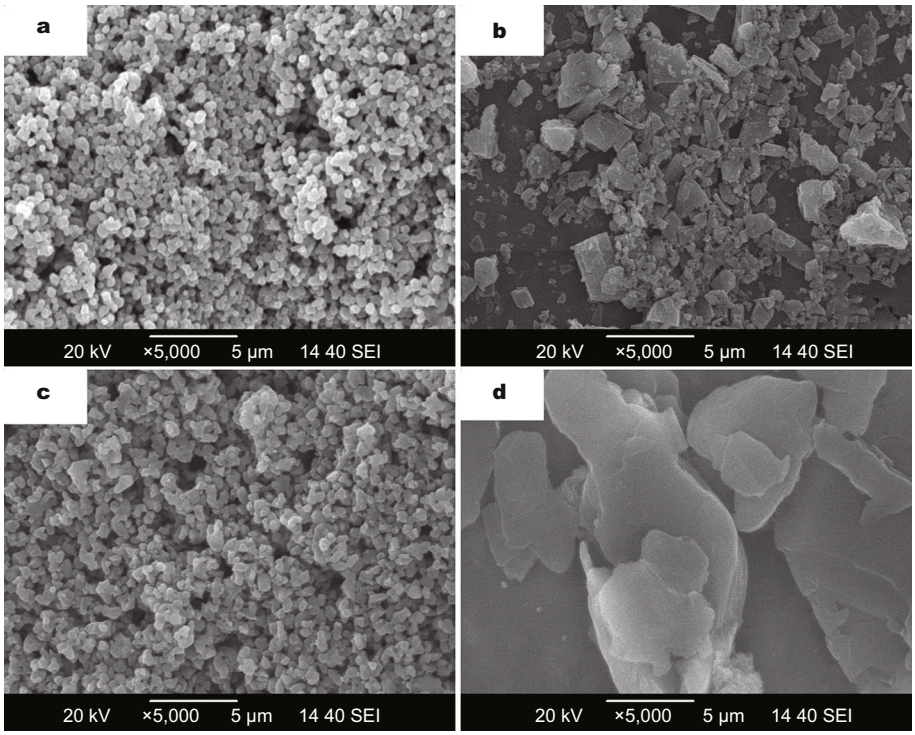

Figure 3 SEM images of (a) LNCM, (b) Cr_2O_5, (c) LTO and (d) graphite.

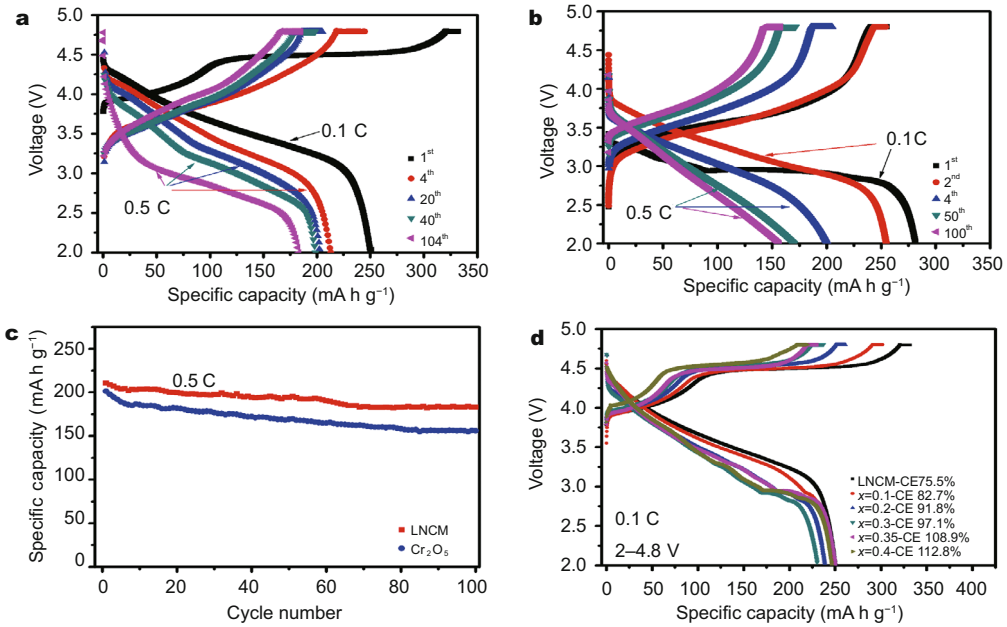

Figure 4 The electrochemical properties of several cathode materials: (a) the selected charge-discharge curves of LNCM at 0.1 and 0.5 C; (b) the selected charge-discharge curves of Cr_2O_5 at 0.1 and 0.5 C; (c) the cycling performances of LNCM and Cr_2O_5 at 0.5 C; (d) the first charge-discharge curves of LNCM@Cr_2O_5 composites with different x values.

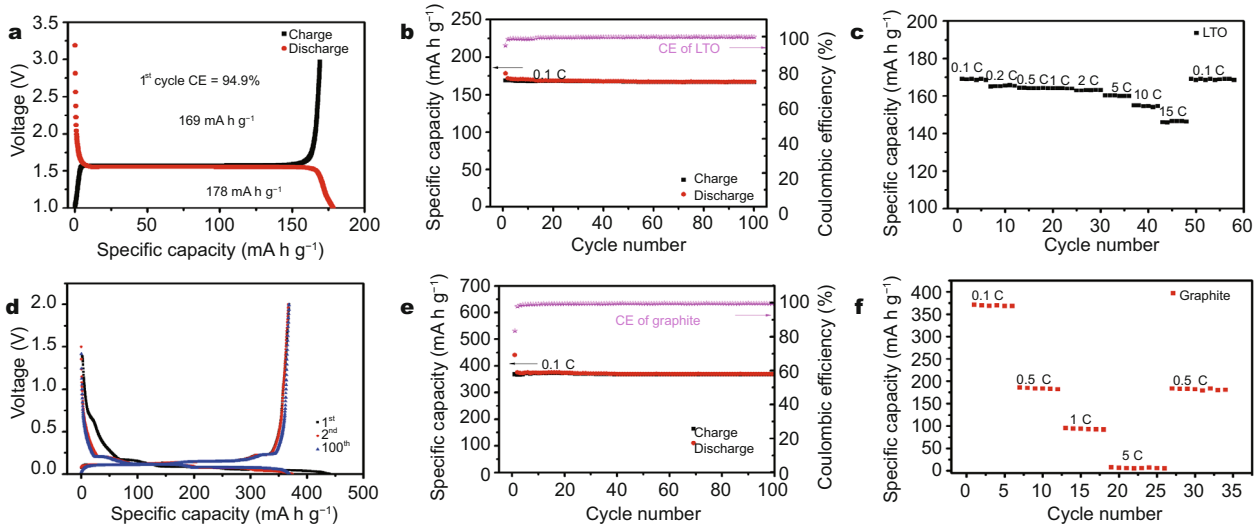

Figure 5 (a) The 1st charge-discharge curve of LTO at 0.1 C (1.0–3.0 V, 1 C = 175 mA h g^{-1}); (b) the cycling performance of LTO at 0.1 C; (c) the rate performance of LTO at different charge rates (1 C discharge); (d) the selected cycle curves of graphite at 0.1 C (0–2V, 1 C = 372 mA h g^{-1}); (e) the cycling performance of graphite at 0.1 C; (f) the rate performance of graphite at different charge rates (1 C discharge).

specific capacities are 250, 210, 189, 133 and 77 mA h g^{-1} at 0.1, 0.5, 1, 5 and 10 C discharge current densities (but the same charge current density of 1 C, Fig. S3a), respectively, which benefits from the uniform nanoscale particles (400 nm) of LNCM. The electrochemical performance of the synthesized Cr_2O_5 in a half-cell (2.0–4.8 V *vs.* Li) is shown in Fig. 4b, c. From Fig. 4b, it is able to transmit discharge-charge capacities of 282 and 255 mA h g^{-1} with a 90% ICE at 0.1 C. In this case, 10% Li^+ loss is ascribed to the formation of a lithiated phase $Li_yCr_2O_5$ in the first discharge step according to our previous study [35]. This $Li_yCr_2O_5$ phase can be cycled reversibly between $Li_yCr_2O_5$ and $Li_{y/10}Cr_2O_5$ in the subsequent cycles. As a result, the coulombic efficiency of Cr_2O_5 is all close to 100% in the subsequent cycles. The specific capacity is 201 mA h g^{-1} at 0.5 C initially and 157 mA h g^{-1} remained after 100 cycles with a 78% capacity retention (Fig. 4c). The rate capability of Cr_2O_5 cathode is shown in Fig. S3b, which demonstrates that the reversible capacities of Cr_2O_5 are 255, 201, 175 and 68 mA h g^{-1} at 0.1 C, 0.5 C, 1 C and 5 C discharge current densities (1 C charge current density), respectively. Furthermore, the first cycles of composite electrodes LNCM@Cr_2O_5 (2.0–4.8 V *vs.* Li) with different x values are shown in Fig. 4d. The ICE is improved from 75.5% to 82.7%, 91.8%, 97.1%, 108.9% and 112.8% with increasing the x value to 0.1, 0.2, 0.3, 0.35 and 0.4, respectively. Specifically, the charge-discharge capacities of LNCM@Cr_2O_5 are 302 and 250 (x = 0.1); 261 and 239 (x = 0.2); 237 and 230 (x = 0.3); 230 and 251 (x = 0.35); 220 and 246 mA h g^{-1} (x = 0.4), respectively. The 2.8 V plateau region is connected with Cr_2O_5 lithiation during the first discharge process according to the previous research in our group [35]. The results demonstrate that the LNCM@Cr_2O_5 composite with x = 0.35 indeed provides more appropriate coulombic efficiency and predominant discharge capacity. Therefore, the as-prepared LNCM@Cr_2O_5 (x = 0.35) composite cathode was adopted to be matched with LTO anode to construct a full cell.

The electrochemical performances of the as-prepared LTO and graphite anodes are shown in Fig. 5. The charge-discharge capacities of LTO (Fig. 5a–c) at 0.1 C are 169 and 178 mA h g^{-1} with a 94.9% ICE. The capacity retention of LTO is 98.6% during 100 cycles. Moreover, LTO can deliver rate capacities of 169, 165, 164, 163, 160, 155, 146 mA h g^{-1} at 0.1, 0.2, 1, 2, 5, 10 and 15 C, which is much superior to the rate performance of graphite (Fig. 5f). As for graphite (Fig. 5d–f), the charge-discharge capacities are 368 and 440 mA h g^{-1} at 0.1 C with an ICE of 83.6% and the capacity retention is 99.9% during 100 cycles, but the rate performances of graphite are 368, 185, 95, 7 mA h g^{-1} at 0.1, 0.5, 1 and 5 C. Hence, graphite is not competitive compared to LTO at high rate charge process in half-cell. Satisfyingly, both of graphite and LTO anodes have almost perfect cycling stability with just insignificant capacity fading during 100 cycles. So a good cycling stability can be expected for the designed LNCM@Cr_2O_5//LTO and LNCM//graphite full-cell.

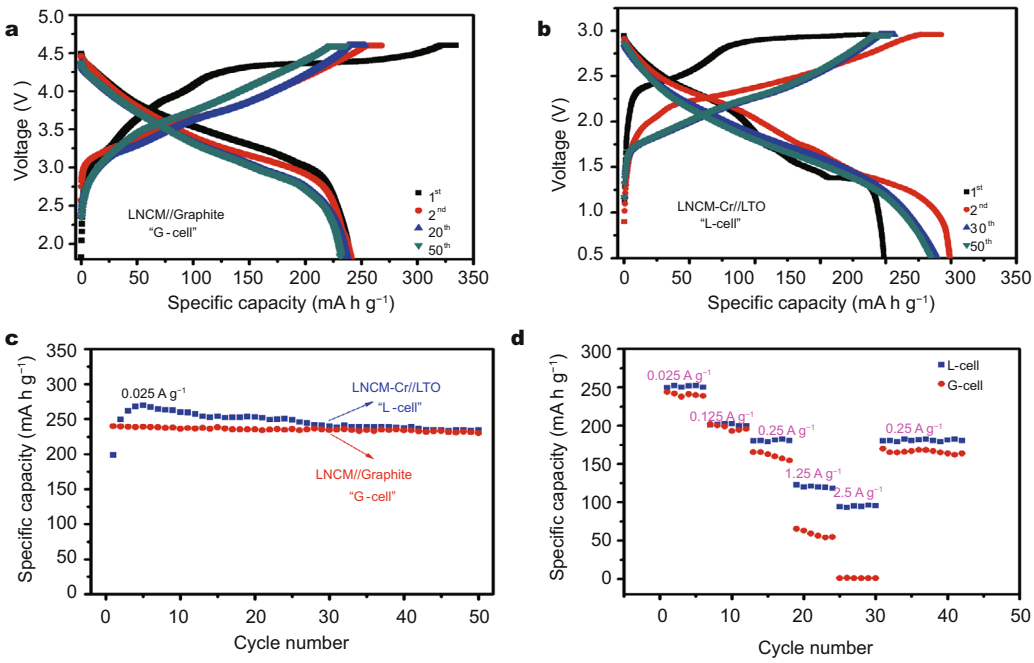

Figure 6 (a) The selected charge and discharge curves of "G-cell" at a current density of 0.025 A g^{-1} (1.8–4.6 V); (b) the selected charge and discharge curves of "L-cell" at a current density of 0.025 A g^{-1} (0.5–2.96 V); (c) the cycling performances of "G-cell" and "L-cell" at a current density of 0.025 A g^{-1}; (d) the rate performances of "G-cell" and "L-cell" at different discharge rates (0.25 A g^{-1} charge).

After the above optimization, the LNCM@Cr_2O_5 (x = 0.35) and LTO are adopted as the cathode and anode to assemble a full cell, i.e., LNCM@0.35Cr_2O_5//LTO ("L-cell"). Simultaneously, for comparison with the "L-cell", this LNCM and graphite are also chosen to assemble a full cell, i.e., LNCM//graphite ("G-cell"). The capacities of both full-cells are controlled by cathodes. The specific capacities of the "G-cell" are 334 and 241 mA h g^{-1} with an ICE of 71.8% in charge-discharge process and the discharge capacity is 231 mA h g^{-1} remained after 50 cycles with a capacity retention of 95.8% (Fig. 6a, c). In this case, the necessary SEI film formed on graphite electrode in the first cycle is from the consuming of excess lithium from the Li-rich cathode. The specific capacities of the "L-cell" are 203.5 and 198.8 mA h g^{-1} with a 97.7% ICE in charge-discharge process and the second charge-discharge capacities are 243 and 249 mA h g^{-1} with a coulombic efficiency of 102% (Fig. 6b). The coulombic efficiencies are above 100% in the subsequent cycles possibly due to the dual-ion battery effect of Cr_2O_5 [36–38]. In the first two cycles, the charge curves correspond to the activation of Li_2MnO_3 phase and the initial charge-discharge capacity are relatively lower than that in the half-cell just because of the twice activation (Fig. 6b), while there is only once activation in the LNCM//lithium half-cell (Fig. 4a). It has to be explained that the relatively low charging upper limit voltage (2.96 V) results in incomplete activation of L-rich@0.35Cr_2O_5 cathode just after the 1st cycle in the "L-cell". The discharge capacities are 249 and 252 mA h g^{-1} in the 2nd and 3rd cycles and keep stable in the subsequent cycles, which is much higher than the capacity in the first cycle (Fig. S4a). Moreover, only after the 1st cycle, the diffraction peaks of Li_2MnO_3 still exist although with decreases in intensity, but the Li_2MnO_3 diffraction peaks disappear after the 2nd cycle of the "L-cell" (Fig. S4b). The capacity is still 234 mA h g^{-1} remained after 50 cycles with a capacity retention as high as 94% after the activation cycle (Fig. 6c). This result obviously illustrates that the excess lithium is effectively used electrochemically by the Li-lacking Cr_2O_5 in the composite cathode in each cycle. The average discharge voltage and specific energy of the "L-cell" are 1.99 V and 500 W h kg^{-1} at a charge-discharge current density of 0.025 A g^{-1} (based on the cathode mass), which appears lower than 3.36 V and 806 W h kg^{-1} obtained from the "G-cell" at the same charge-discharge current density (Fig. 6c) due to the relatively high voltage plateau of LTO anode. However, when cycling at higher current densities of 0.25, 1.25 and 2.5 A g^{-1}, the "L-cell" can deliver specific capacities as high as 180, 122 and 94 mA h g^{-1}, respec-

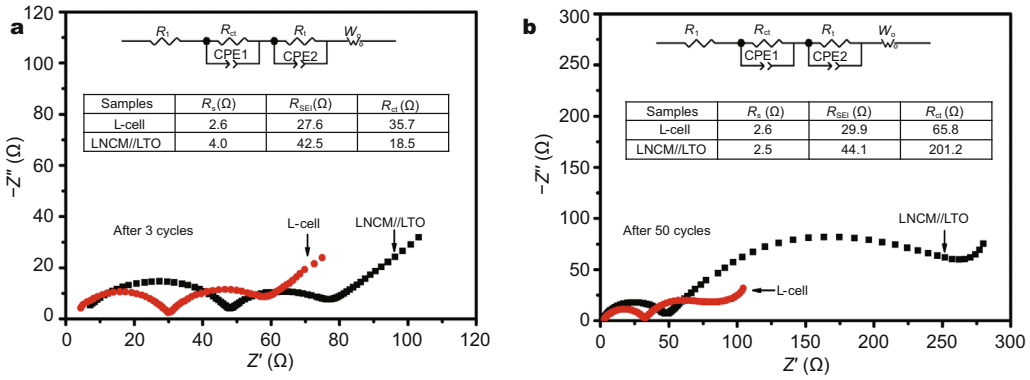

Figure 7 EIS of the LNCM//LTO full-cell and "L-cell" (a) after 3 cycles and (b) after 50 cycles at discharged state of 2.3 V.

tively (Fig. 6d and Fig. S5), while it is only 165, 65, and 1 mA h g^{-1} for the "G-cell", respectively (Fig. 6d). Based on this, the energy densities of the "L-cell" are 225 and 153 W h kg^{-1} at discharge current densities of 1.25 and 2.5 A g^{-1}, respectively, which are only 143 and 20 W h kg^{-1} for the "G-cell". Moreover, the cycling performance of LNCM//LTO full cell was also tested as a comparative of the "L-cell" (Fig. S6). The LNCM//LTO full cell can deliver a specific capacity of 226 mA h g^{-1} with a capacity retention of 76.2% during 50 cycles at the current density of 0.025 A g^{-1}, which is much inferior compared with the "L-cell". Therefore, the "L-cell" exhibits much superior rate performance and higher energy densities at high current densities, indicating significant potential of being applied to fast charge-discharge field in future high-energy batteries for EVs/HEVs.

The Nyquist plots and the equivalent circuits of the LNCM//LTO full cell and "L-cell" after 3 and 50 cycles are shown in Fig. 7a, b, respectively. In general, the intercept on the *x*-axis is corresponding to the impedance of electrolyte (R_s). The two semicircles in the high-frequency and medium-frequency regions refer to the charge transfer resistance (R_{ct}) and the resistance of the SEI layers (R_t or R_{SEI}), respectively. The straight line in the low-frequency is connected with the Warburg impedance (W_o). The values of R_s for the two full cells are all at 2.5–4 Ω after 3 and 50 cycles. The R_{ct} for LNCM//LTO full cell changes slightly from 42.5 to 44.1 Ω after 50 cycles. Likewise, the R_{ct} for the "L-cell" increases slightly from 27.6 to 29.9 Ω after 50 cycles. However, the R_{SEI} of the 50 times-cycled LNCM//LTO full cell increases from 18.5 to 201.2 Ω, which is only an increase from 35.7 to 65.8 Ω for the "L-cell". The increase of the R_{SEI} values demonstrate the continual decomposition of electrolyte and formation of the unfavorable SEI film during the full-cells cycling process. Thus, the Li-lacking Cr_2O_5 in the composite cathode material probably suppress the electrolyte decomposition by utilizing the extra Li^+ in Li-rich cathode so as to alleviate the dissolution of Mn^{2+} [39], which can catalyze the decomposition of electrolyte. The consequence displays that the "L-cell" indeed provides better cycling stability than LNCM//LTO full cell.

In order to further confirm that Cr_2O_5 exactly makes use of the extra irreversible Li^+ from Li-rich cathode, *ex-situ* XRD was used to study the structural change during the first charge-discharge process of Li^+ insertion/extraction in LNCM@Cr_2O_5 cathode. For Li-rich cathode in half cell, the peaks located at 20° to 25° disappear after the first cycle (Fig. 8, A1), which is considered to be irreversible transformation of Li_2MnO_3 phase from layered-structure to spinel-structure $LiMn_2O_4$.

As shown in Fig. 8, after the first cycle of Cr_2O_5 cathode (pattern A2) and LNCM@0.35Cr_2O_5 composite cathode (pattern A3) in half cells, two new diffraction peaks (220)

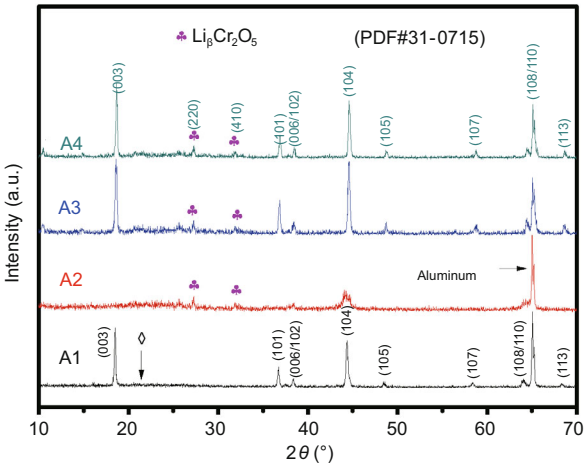

Figure 8 *Ex-situ* XRD of first cycled, A1: Li-rich cathode in half cell; A2: Cr_2O_5 cathode in half cell; A3: LNCM@0.35Cr_2O_5 composite cathode in half cell; A4: LNCM@0.35Cr_2O_5 composite cathode in "L-cell".

and (410) corresponding to $Li_\beta Cr_2O_5$ compounds (PDF#31-0715) are observed, indicating that lithium ions have been intercalated into Cr_2O_5 to form $Li_\beta Cr_2O_5$, in which the β value changes along with the charge-discharge process. In detail, according to the study in Feng's paper [35], the β value of $Li_\beta Cr_2O_5$ is 1.7 if fully discharged. It has to be mentioned that the Li^+ in $Li_\beta Cr_2O_5$ is either originally from the Li-rich cathode or from the lithium metal anode. Therefore, *ex-situ* XRD of the first cycled LNCM-0.35Cr_2O_5 composite cathode in "L-cell" was also conducted (Fig. 8, pattern A4). Two new diffraction peaks (220) and (410) appear just like that in half cell, which exactly proves that the extra irreversible Li^+ from Li-rich cathode can be effectively stored in Cr_2O_5 structure to form $Li_\beta Cr_2O_5$ compounds in "L-cell".

CONCLUSIONS

In summary, Li-rich LNCM, Cr_2O_5 and LNCM-xCr_2O_5 (x = 0, 0.1, 0.2, 0.3, 0.35, 0.4, mass ratio) with satisfactory electrochemical performance were synthesized. After electrochemical tests, LNCM@0.35Cr_2O_5 and $Li_4Ti_5O_{12}$ were picked as the optimized cathode and anode electrodes to fabricate a full cell ("L-cell"). According to the coulombic efficiency accordance and capacity equivalence mechanism, such an "L-cell" demonstrates particularly high ICE as high as 97.7%, excellent cycling and rate performances and higher energy density, which is superior to the "G-cell" for potential fast charge-discharge applications in EVs/ HEVs. This novel idea to solve the low ICE problem of Li-rich cathode should be taken seriously. Much better performance can be expected for Li-ion batteries with the improvement of design and fabrication process.

Received 19 June 2017; accepted 24 July 2017; published online 30 August 2017

1 Chu S, Majumdar A. Opportunities and challenges for a sustainable energy future. Nature, 2012, 488: 294–303
2 Yi TF, Han X, Yang SY, *et al.* Enhanced electrochemical performance of Li-rich low-Co $Li_{1.2}Mn_{0.56}Ni_{0.16}Co_{0.08-x}Al_xO_2$ ($0\le x\le 0.08$) as cathode materials. Sci China Mater, 2016, 59: 618–628
3 Dunn B, Kamath H, Tarascon JM. Electrical energy storage for the grid: a battery of choices. Science, 2011, 334: 928–935
4 Zeng L, Pan A, Liang S, *et al.* Novel synthesis of V_2O_5 hollow microspheres for lithium ion batteries. Sci China Mater, 2016, 59: 567–573
5 Hao J, Liu H, Ji Y, *et al.* Synthesis and electrochemical performance of Sn-doped $LiNi_{0.5}Mn_{1.5}O_4$ cathode material for high-voltage lithium-ion batteries. Sci China Mater, 2017, 60: 315–323
6 Padhi AK. Phospho-olivines as positive-electrode materials for rechargeable lithium batteries. J Electrochem Soc, 1997, 144: 1188–1194
7 Zou BK, Ma XH, Tang ZF, *et al.* High rate $LiMn_2O_4$/carbon nanotube composite prepared by a two-step hydrothermal process. J Power Sources, 2014, 268: 491–497
8 Wu N, Wu H, Yuan W, *et al.* Facile synthesis of one-dimensional $LiNi_{0.8}Co_{0.15}Al_{0.05}O_2$ microrods as advanced cathode materials for lithium ion batteries. J Mater Chem A, 2015, 3: 13648–13652
9 Johnson CS, Kim JS, Lefief C, *et al.* The significance of the Li_2MnO_3 component in 'composite' $xLi_2MnO_3\cdot(1-x)LiMn_{0.5}Ni_{0.5}O_2$ electrodes. Electrochem Commun, 2004, 6: 1085–1091
10 Johnson CS, Li N, Lefief C, *et al.* Synthesis, characterization and electrochemistry of lithium battery electrodes: $xLi_2MnO_3\cdot(1-x)LiMn_{0.333}Ni_{0.333}Co_{0.333}O_2$ ($0\le x\le 0.7$). Chem Mater, 2008, 20: 6095–6106
11 Shi JL, Zhang JN, He M, *et al.* Mitigating voltage decay of Li-rich cathode material *via* increasing Ni content for lithium-ion batteries. ACS Appl Mater Interfaces, 2016, 8: 20138–20146
12 Martha SK, Nanda J, Veith GM, *et al.* Electrochemical and rate performance study of high-voltage lithium-rich composition: $Li_{1.2}Mn_{0.525}Ni_{0.175}Co_{0.1}O_2$. J Power Sources, 2012, 199: 220–226
13 Wu Y, Vadivel Murugan A, Manthiram A. Surface modification of high capacity layered $Li[Li_{0.2}Mn_{0.54}Ni_{0.13}Co_{0.13}]O_2$ cathodes by $AlPO_4$. J Electrochem Soc, 2008, 155: A635
14 Xu H, Deng S, Chen G. Improved electrochemical performance of $Li_{1.2}Mn_{0.54}Ni_{0.13}Co_{0.13}O_2$ by Mg doping for lithium ion battery cathode material. J Mater Chem A, 2014, 2: 15015–15021
15 Zhang X, Belharouak I, Li L, *et al.* Structural and electrochemical study of Al_2O_3 and TiO_2 coated $Li_{1.2}Ni_{0.13}Mn_{0.54}Co_{0.13}O_2$ cathode material using ALD. Adv Energ Mater, 2013, 3: 1299–1307
16 Liu J, Reeja-Jayan B, Manthiram A. Conductive surface modification with aluminum of high capacity layered $Li[Li_{0.2}Mn_{0.54}Ni_{0.13}Co_{0.13}]O_2$ cathodes. J Phys Chem C, 2010, 114: 9528–9533
17 Zheng F, Yang C, Xiong X, *et al.* Nanoscale surface modification of lithium-rich layered-oxide composite cathodes for suppressing voltage fade. Angew Chem Int Ed, 2015, 54: 13058–13062
18 Lee E, Park JS, Wu T, *et al.* Role of Cr^{3+}/Cr^{6+} redox in chromium-substituted $Li_2MnO_3\cdot LiNi_{1/2}Mn_{1/2}O_2$ layered composite cathodes: electrochemistry and voltage fade. J Mater Chem A, 2015, 3: 9915–9924
19 He Z, Wang Z, Chen H, *et al.* Electrochemical performance of zirconium doped lithium rich layered $Li_{1.2}Mn_{0.54}Ni_{0.13}Co_{0.13}O_2$ oxide with porous hollow structure. J Power Sources, 2015, 299: 334–341
20 Qiao QQ, Qin L, Li GR, *et al.* Sn-stabilized Li-rich layered Li$(Li_{0.17}Ni_{0.25}Mn_{0.58})O_2$ oxide as a cathode for advanced lithium-ion batteries. J Mater Chem A, 2015, 3: 17627–17634
21 Sun S, Wan N, Wu Q, *et al.* Surface-modified $Li[Li_{0.2}Ni_{0.17}Co_{0.07}Mn_{0.56}]O_2$ nanoparticles with MgF_2 as cathode for Li-ion battery. Solid State Ion, 2015, 278: 85–90
22 Yu H, Zhou H. High-energy cathode materials (Li_2MnO_3-$LiMO_2$) for lithium-ion batteries. J Phys Chem Lett, 2013, 4: 1268–1280
23 Gao J, Kim J, Manthiram A. High capacity $Li[Li_{0.2}Mn_{0.54}Ni_{0.13}Co_{0.13}]O_2$-$V_2O_5$ composite cathodes with low irreversible capacity loss for lithium ion batteries. Electrochem Commun, 2009, 11: 84–86
24 Wu F, Wang Z, Su Y, *et al.* $Li[Li_{0.2}Mn_{0.54}Ni_{0.13}Co_{0.13}]O_2$-$MoO_3$ composite cathodes with low irreversible capacity loss for lithium ion batteries. J Power Sources, 2014, 247: 20–25
25 Liu JL, Wang J, Xia YY. A new rechargeable lithium-ion battery with a $xLi_2MnO_3\cdot(1-x)LiMn_{0.4}Ni_{0.4}Co_{0.2}O_2$ cathode and a hard carbon anode. Electrochim Acta, 2011, 56: 7392–7396

26 Wang T, Chen Z, Zhao R, *et al.* A new high energy lithium ion batteries consisting of $0.5Li_2MnO_3{\cdot}0.5LiMn_{0.33}Ni_{0.33}Co_{0.33}O_2$ and soft carbon components. Electrochim Acta, 2016, 194: 1–9
27 Pham HQ, Hwang EH, Kwon YG, *et al.* Understanding the interfacial phenomena of a 4.7 V and 55°C Li-ion battery with Li-rich layered oxide cathode and graphite anode and its correlation to high-energy cycling performance. J Power Sources, 2016, 323: 220–230
28 Zou B, Hu Q, Qu D, *et al.* A high energy density full lithium-ion cell based on specially matched coulombic efficiency. J Mater Chem A, 2016, 4: 4117–4124
29 Elia GA, Wang J, Bresser D, *et al.* A new, high energy Sn–C/Li $[Li_{0.2}Ni_{0.4/3}Co_{0.4/3}Mn_{1.6/3}]O_2$ lithium-ion battery. ACS Appl Mater Interfaces, 2014, 6: 12956–12961
30 Li M, Hou X, Sha Y, *et al.* Facile spray-drying/pyrolysis synthesis of core–shell structure graphite/silicon-porous carbon composite as a superior anode for Li-ion batteries. J Power Sources, 2014, 248: 721–728
31 Ren JG, Wu QH, Hong G, *et al.* Silicon-graphene composite anodes for high-energy lithium batteries. Energ Tech, 2013, 1: 77–84
32 Leroy S, Blanchard F, Dedryvère R, *et al.* Surface film formation on a graphite electrode in Li-ion batteries: AFM and XPS study. Surf Interface Anal, 2005, 37: 773–781
33 Xu B, Fell CR, Chi M, *et al.* Identifying surface structural changes in layered Li-excess nickel manganese oxides in high voltage lithium ion batteries: a joint experimental and theoretical study. Energ Environ Sci, 2011, 4: 2223–2233
34 Yabuuchi N, Yoshii K, Myung ST, *et al.* Detailed studies of a high-capacity electrode material for rechargeable batteries, $Li_2MnO_3-LiCo_{1/3}Ni_{1/3}Mn_{1/3}O_2$. J Am Chem Soc, 2011, 133: 4404–4419
35 Feng XY, Ding N, Wang L, *et al.* Synthesis and reversible lithium storage of Cr_2O_5 as a new high energy density cathode material for rechargeable lithium batteries. J Power Sources, 2013, 222: 184–187
36 Beltrop K, Meister P, Klein S, *et al.* Does size really matter? New insights into the intercalation behavior of anions into a graphite-based positive electrode for dual-ion batteries. Electrochim Acta, 2016, 209: 44–55
37 Rothermel S, Meister P, Schmuelling G, *et al.* Dual-graphite cells based on the reversible intercalation of bis(trifluoromethanesulfonyl)imide anions from an ionic liquid electrolyte. Energ Environ Sci, 2014, 7: 3412–3423
38 Balabajew M, Reinhardt H, Bock N, *et al. In-situ* Raman study of the intercalation of bis(trifluoromethylsulfonyl)imid ions into graphite inside a dual-ion cell. Electrochim Acta, 2016, 211: 679–688
39 Choi NS, Han JG, Ha SY, *et al.* Recent advances in the electrolytes for interfacial stability of high-voltage cathodes in lithium-ion batteries. RSC Adv, 2015, 5: 2732–2748

Acknowledgements This work was supported by the National Natural Science Foundation of China (51577175), and NSAF (U1630106). We are also grateful to Elementec Ltd. in Suzhou for its technical support.

Author contributions Ding X performed the main experiments; He X and Liao J participated in the characterization. Zou B, Li Y, Tang Z and Shao Y conceived and supervised the project; Ding X wrote the manuscript with support from Chen C, Zou B, Tang Z. All authors contributed to the general discussion.

Conflict of interest The authors declare that they have no conflict of interest.

Supplementary information Supporting data are available in the online version of the paper.

Xiang Ding received his bachelor degree from Jilin University (JLU) in 2015. He is currently pursuing his master degree under the supervision of Prof. Chunhua Chen at the Institute for CAS Key Laboratory of Materials for Energy Conversions, University of Science and Technology of China (USTC). His research interests are the materials for rechargeable lithium ion batteries.

Chunhua Chen is a professor of the Department of Materials Science and Engineering at USTC. He graduated from USTC in 1986 and received his master degree at USTC in 1989. He obtained his PhD degree at Delft University of Technology (TUD), Netherlands, in 1998. Then he worked in Argonne National Laboratory (ANL), USA, until 2002. His research interest focuses on the materials and systems for secondary batteries. He has published more than 200 research papers with a current H-index of 46.

富锂相@五氧化二铬复合正极和锂钛氧负极匹配的具有可控库仑效率新型锂离子电池

丁翔, 邹邦坤, 李禹宣, 贺晓东, 廖家英, 唐仲丰, 邵宇, 陈春华*

摘要 本文将缺锂态的Cr_2O_5正极材料与$Li_{1.2}Ni_{0.13}Co_{0.13}Mn_{0.54}O_2$(LNCM)富锂相正极材料进行物理混合, 形成了复合正极材料LNCM@$x$$Cr_2O_5$($x$ = 0,0.1,0.2,0.3,0.35, 0.4), 从而在第一次充放电过程中达到有效利用富锂相所产生的不可逆的锂离子. 复合之后, LNCM半电池的首次库仑效率(ICE)得到显著提高, 从75.5(x = 0)提高到了108.9(x = 0.35). LNCM@Cr_2O_5复合正极材料和$Li_4Ti_5O_{12}$负极材料匹配而成的新型锂离子全电池, 即LNCM@Cr_2O_5//$Li_4Ti_5O_{12}$("L电池")表现出高达97.7的ICE. 不仅如此, "L电池"还表现出了高达250 mA h g^{-1}的可逆容量, 并且在循环50次之后仍具有94%的容量保持率. 此外, 在1.25和2.5 A g^{-1}电流密度下, 它还具有高达122和94 mA h g^{-1}的放电比容量, 远远优于LNCM//石墨全电池("G电池"). "L电池"的高性能得益于精心设计的库仑效率匹配机制, 并且在未来高能量锂离子电池的快速充放电应用中表现出巨大的潜力.